Schottkey barrier measurement of nanocrystalline Lu3N@ C80/Au contac

doi: info:doi/10.4236/msa.2013.412103

Materials Sciences and Applications, 2013, 4, 808-815
Published Online December 2013 (http://www.scirp.org/journal/msa)
http://dx.doi.org/10.4236/msa.2013.412103

Scientific Research

Schottkey Barrier Measurement of Nanocrystalline $Lu_3N@C_{80}$/Au Contact

Yong Sun[1*], Yusuke Hattori[1], Masamichi Sakaino[1], Fumio Morimoto[2], Kenta Kirimoto[3]

[1]Department of Applied Science for Integrated System Engineering, Kyushu Institute of Technology, Fukuoka, Japan; [2]Research Institute, Kyushu Kyoritsu University, Fukuoka, Japan; [3]Department of Electrical and electronic Engineering, Kitakyushu National College of Technology, Fukuoka, Japan.
Email: *sun@ele.kyutech.ac.jp

Received October 21, 2013; revised November 28, 2013; accepted December 9, 2013

ABSTRACT

Electrical and structural properties of nanocrystalline solids of C_{80} fullerene encapsulated with a Lu_3N cluster, $Lu_3N@C_{80}$, have been studied by measuring x-ray photoemission spectra, x-ray diffraction, and current-voltage characteristics of the $Lu_3N@C_{80}$/Au Schottky contact in the temperature range of 300 - 500 K. The nanocrystalline solid sample of $Lu_3N@C_{80}$ fullerene consists of grains characterized with an fcc structure and those grains become larger in size after pressing the powder sample at 1.25 GPa. The current-voltage characteristics measured at various temperatures showed that there are no significant dependences on both the Schottky barrier and the carrier mobility on electric field. The Schottky barrier of the $Lu_3N@C_{80}$/Au contact is determined to be 0.71 ± 0.04 eV.

Keywords: $Lu_3N@C_{80}$; Nanocrystalline; Schottky Barrier; Mobility

1. Introduction

Higher fullerenes of C_{80} are promising agent for organic photovoltaic devices particularly when they encapsulate a M_3N cluster (M: Sc, Lu, Er, Dy, Y, Ho, La, Tm, Gd, etc.) inside the C_{80} cage. The recent isolation technique has succeeded in isolating those M_3N endohedral C_{80} fullerenes, $M_3N@C_{80}$, with a production yield more than ten times higher than other endohedral metallofullerenes [1-4]. Electron transfer from a M_3N cluster to the C_{80} cage as well as the specific charge states of both the cluster and cage is of special interest in photovoltaic solar cells. Bare C_{80} fullerenes that satisfy the isolated pentagon rule (IPR) [5] have seven isomers [6] with symmetries of I_h, D_{5d}, D_{5h}, D_3, D_2, C_{2v} and C_{2v}, among which only the D_2 and D_{5d} isomers are able to be isolated because of their structural stability. It is known that excessive electrons can stabilize the molecular structure of the C_{80} cage, so the $M_3N@C_{80}$ molecules with I_h and D_{5h} symmetries can also be obtained [7]. Also, the molecules with the excessive electrons from the endohedral cluster can interact with metal electrodes so that contact resistance at the metal/$M_3N@C_{80}$ interface is reduced [8]. Furthermore, it is reported that the endohedral M_3N cluster influences the carrier transport since the current through the Al/$M_3N@C_{80}$/Al system is obtained to be two times larger than that for the Al/C_{80}/Al system [8].

With all the expectations for the promising abilities of $M_3N@C_{80}$ fullerenes for electronic, magnetic and optical devices, their solid state properties have not been well understood, yet. So far, all the theoretical and experimental studies have focused mainly on the chemical and physical properties of an isolated single $M_3N@C_{80}$ molecule, treating structure of the isomers [6,9], HOMO-LUMO energy gap [1,6], bond energy [6], electronic structure of neutral as well as ionized molecules [10], molecular dynamics [11,12], superatom [13], size effects of the endohedral clusters[14], magnetic moment [15,16], and optical and electrochemical properties [11,17].

In this study, we have prepared nanocrystalline $Lu_3N@C_{80}$ solids, and revealed their properties about crystallographic structure, oxygen-induced chemical shifts of the core levels of constituting atoms, and effect of applied electric field on the Schottky barrier and the carrier mobility. Schottky barrier of the nanocrystalline $Lu_3N@C_{80}$/Au contact is evaluated from the temperature-dependent current passing through the sample.

*Corresponding author.

2. Experimental

Solid samples were prepared using $Lu_3N@C_{80}$ powder (purity > 97 wt%) purchased from LUNA Innovations. The $Lu_3N@C_{80}$ powder was pressed into a pellet with two gold electrodes at room temperature at a pressure of 1.25 GPa for 50 min. The so formed pellet was 5 mm in diameter and 0.525 mm thick. Prior to the measurements the powder and pellet samples were characterized by field emission scanning electron microscope (FE-SEM, JEOL JSM-7000), x-ray photoemission spectroscopy (XPS; AXIS-NOVA, SHIMATSU/KRATOS) and x-ray diffraction (XRD; JEOL JDX-3500K). In the XPS analysis the beam diameter of Al Kα line was 55 μm, and the binding energy resolution was 0.15 eV.

In the electrical measurements, the current passing through the pellet sample were measured using a digital electrometer (ADVANTEST R8252) with a current resolution of 1 f A at various d.c. bias voltages, V_{bi}, changing from 10 to 200 V. The Au/$Lu_3N@C_{80}$/Au structure consists of two Schottky contacts, connected back-to-back. When a d.c. bias is applied, one of the Schottky diodes is forward and the other is reverse biased. At sufficiently high biases, the Au/$Lu_3N@C_{80}$/Au structure can be considered as a reverse-biased diode. Its current-voltage characteristics can be written as $J = J_0 = A^* T^2 \exp\left(-q\Phi_B / k_B T\right)$ where J_0 is the reverse saturation-current density, A^* the effective Richardson constant, $q\Phi_B$ the Schottky barrier and k_B the Boltzmann constant. Hence, from measurements of the temperature dependent current passing through the sample, $I = AJ$ where A is the area of the electrodes on the sample, the Schottky barrier was obtained.

The pellet sample was set in a vacuum chamber of a cryostat during the electrical measurements. The base pressure of the vacuum chamber was less than 10^{-5} Pa. The current measurements were carried out in the course of heating up or cooling down process between the temperatures from 300 K to 500 K. The rate of heating or cooling was 0.14 $Kmin^{-1}$ with a stepwise increment of 1.0 K.

3. Results

The SEM image of the surface of a $Lu_3N@C_{80}$ pellet sample is shown in **Figure 1**. The inset shows the structure formula of the $Lu_3N@C_{80}$ molecule. **Figure 2** shows three x-ray photoemission spectra of the pellet sample at room temperature. They were obtained from the surface of the $Lu_3N@C_{80}$ sample before and after Ar^+ ion sputtering for 10 and 30 s, respectively. Six peaks at biding energies of 12, 205, 287, 535 and 990 eV were observed in the spectra. The 12 eV peak is attributed to a photoemission from valence electrons of Lu atoms. The double peaks at 200 and 210 eV are the photoemissions from Lu

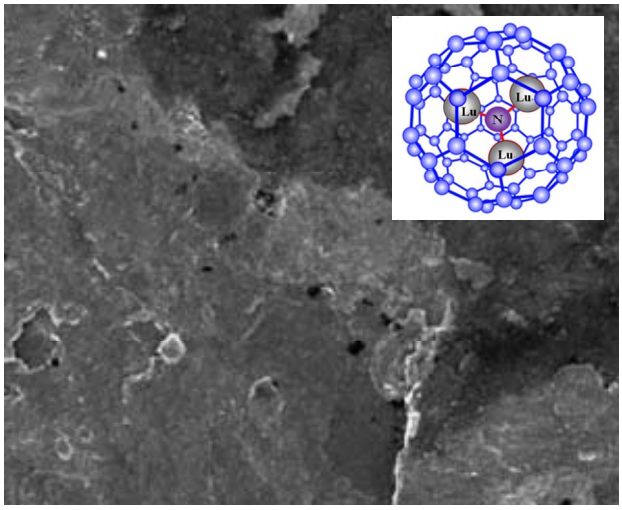

Figure 1. SEM image of the surface of a $Lu_3N@C_{80}$ pellet sample. The inset shows the structure formula of the $Lu_3N@C_{80}$ molecule.

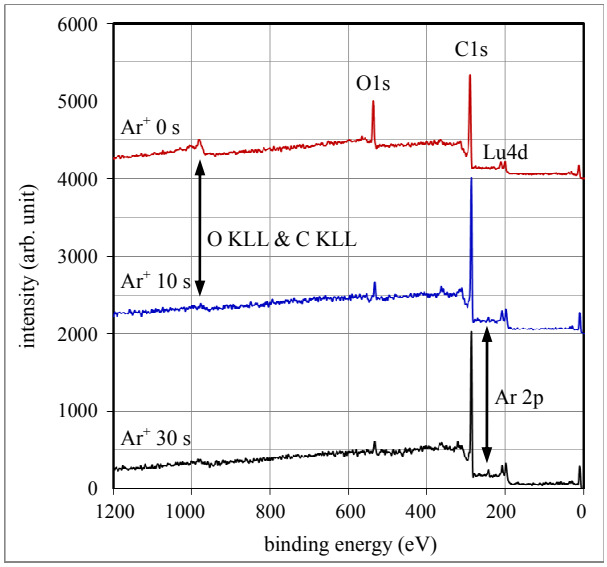

Figure 2. X-ray photoemission spectra of the nanocrystalline $Lu_3N@C_{80}$ sample prepared at a pressure of 1.25 GPa. The spectra are detected on the surface of the sample before and after Ar^+ ion sputtering for 10 and 30 s.

4 $d^{5/2}$ and 4 $d^{3/2}$ core levels. The peak around 287 and 535 eV comes from C 1s and O 1s core level, respectively. The peaks around 990 eV correspond to O KLL and C KVV Auger emissions. Also, the peaks around 240 eV observed after the Ar^+ ion sputtering are from Ar 2 $p^{1/2}$ and 2 $p^{3/2}$ core levers. The measured XPS spectra showed up that the Ar^+ ion sputtering causes both decrease in the O-related peaks and increase in the C and Lu-related peaks. This result indicates that the oxygen atoms adsorb only on the sample surface. From the spectrum after the 30 s Ar^+ ion sputtering, atomic ratio of Lu/C is evaluated to be 3.24 at%, close to the stoichio-

metric ratio of 3.61 at% for $Lu_3N@C_{80}$. One should note that the photoemission from the N 1s level cannot be detected due to its smaller relative sensitivity factor (RSF) of 0.505 compared to the Lu 4 *d* RSF of 2.645. Although the RSF of C 1s is also small, 0.318, the XPS intensity by the C atom is somewhat strong because of the abundant concentration of C atoms in the $Lu_3N@C_{80}$ solid.

The photoemission spectra from the Lu 4 $d^{5/2}$ and 4 $d^{3/2}$ and C 1s core levels were enlarged in the energy scaling and they were respectively plotted in **Figures 3(a)** and **(b)**. The peaks before the Ar^+ ion sputtering appears at binding energies of 211 eV for Lu 4 $d^{3/2}$, 201 eV for Lu 4 $d^{5/2}$ and 289 eV for C 1s core level. On the other hand, the corresponding peaks measured after the sputtering shift to binding energies of 208 eV for Lu 4 $d^{3/2}$,

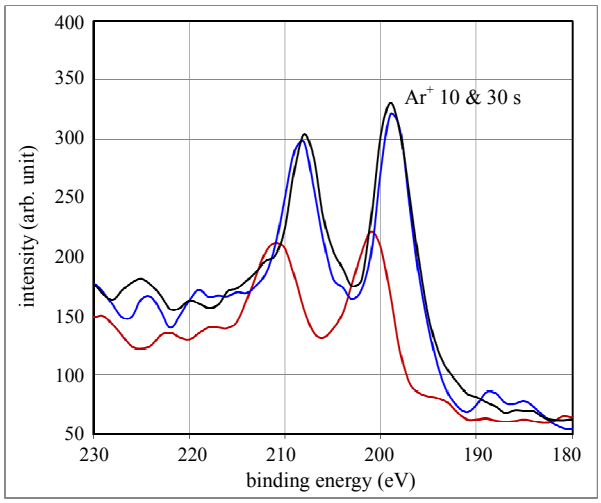

(a)

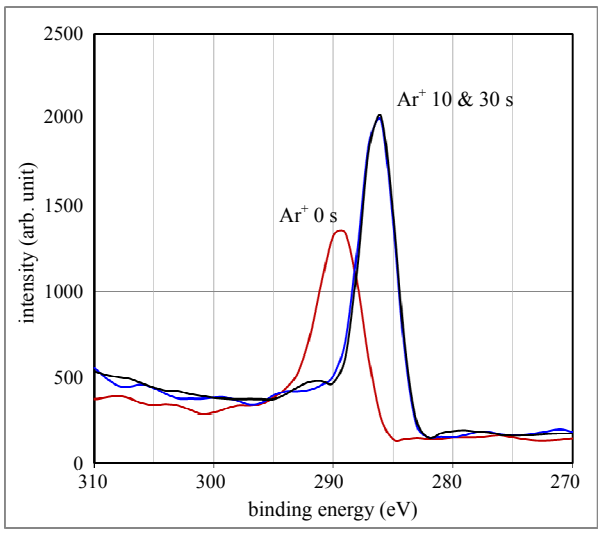

(b)

Figure 3. X-ray photoemission spectra of the nanocrystalline $Lu_3N@C_{80}$ sample before and after Ar^+ ion sputtering for 10 and 30 s, (a) the spectra of Lu 4 $d^{3/2}$ and 4 $d^{5/2}$ core levels and (b) the spectra of C 1s core level.

198 eV for Lu 4 $d^{5/2}$ and 287 eV for C 1s core level. Namely, the binding energies of the core levels shift to the low-energy side after eliminating oxygen adatoms by the Ar^+ ion sputtering. The XPS peak shift is 3.0 eV for the Lu 4 $d^{3/2}$, 3.0 eV for the Lu 4 $d^{5/2}$, and 2.0 eV for the C 1s, respectively. The peak of the Lu valence electrons at 12 eV shifts by 2.0 eV towards the low energy side.

The observed chemical shifts to the lower energy side after the oxygen removal suggest that the oxygen adatoms accept electrons from the valence orbitals of both the C_{80} cage and the endohedral Lu_3N cluster.

Figure 4 shows the XRD patterns of the $Lu_3N@C_{80}$ powder material as-received and the pellet sample prepared by pressing under the pressure of 1.25 GPa. Several diffraction peaks can be recognized for the two patterns, a strong peak at $2\theta = 9.50$ degree and three broad peaks centered at $2\theta = 25.40$, 34.10 and 50.05 degree. The enlarged XRD pattern of the $2\theta = 9.50$ peaks is shown in the inset to **Figure 4**. As seen in the inset figure, three new peaks around the $2\theta = 9.50$ degree appear for the pellet sample after the 1.25 GPa pressing. The $2\theta = 9.50$ peak is ascribed to the diffraction from (111) planes of a fcc grain structure with a lattice constant of 1.61 nm. The grain size of the as-received powder and the pressed pellet sample can be estimated to be 60 and 240 nm from the full width at half-maximum (FWHM) of the (111) peaks. The XRD result suggests that the 1.25 GPa pressing causes not only the regrowth of the fcc grains involved in the powder material with a lattice constant of 1.61 nm but also growth of the new fcc grains characterized with different lattice constants of 1.82 and 1.50 nm.

The current I passing through the pellet sample at V_{bi} =10, 100, 150 and 200 V were measured as a function of temperature T, and the obtained results were plotted in **Figures 5(a)** and **(b)** during heating up and cooling down

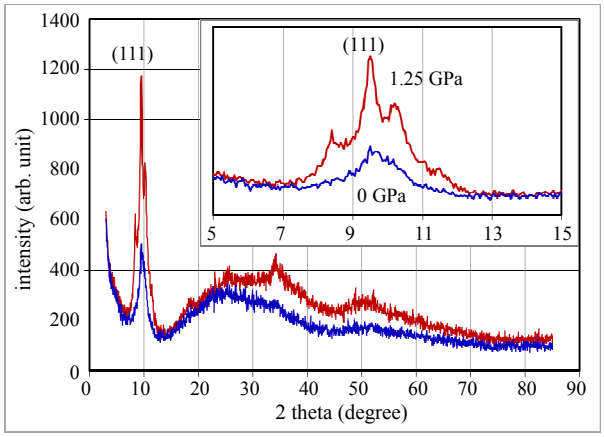

Figure 4. X-ray diffraction patterns of the as-received $Lu_3N@C_{80}$ powder and its pellet sample prepared at a pressure of 1.25 GPa. The inset shows the enlarged patterns of the (111) diffraction peaks.

process, respectively. One may notice that I exponentially increases with T above 400 K. No hysteresis was recognized in the I vs T curves obtained during the heating up and cooling down processes.

Arrhenius plots of $J_0/T^2 = A^* \exp(-q\Phi_B/k_BT)$ at various V_{bi} were shown in **Figures 6(a)** and **(b)** for the measurements during heating up and cooling down process, respectively. The good linear relationship found in the Arrhenius plots in **Figure 6** suggests that carriers are generated by thermal activation over the Schottky barrier $q\Phi_B$. The values of the Schottky barrier were determined as a function of the applied electric field E which were evaluated by a relation $E = V_{bi}/d$ for the sample thickness d. Results during heating up and cooling down were plotted in **Figure 7**. It is clear that the Schottky barrier is constant, not affected by E as well as either by the course of heating up or cooling down process. From **Figure 7** it is determined that $q\Phi_B = 0.71 \pm 0.04$ eV.

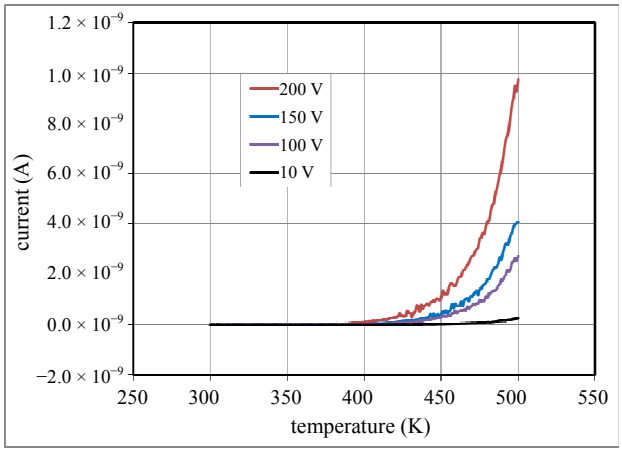

(a)

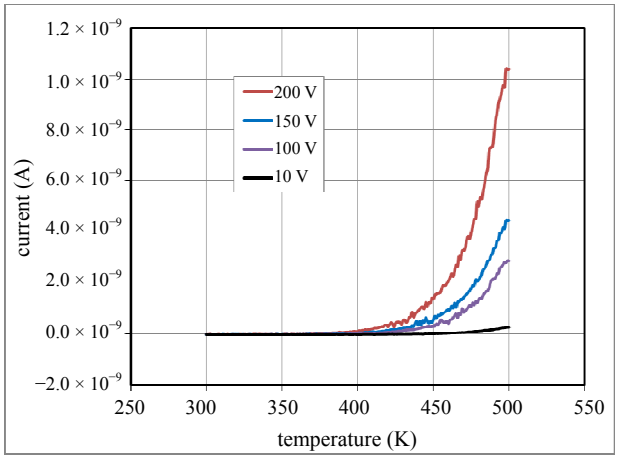

(b)

Figure 5. Temperature-dependent current passing through the nanocrystalline $Lu_3N@C_{80}$ sample at various d.c. bias voltages, (a) during heating up and (b) during cooling down process.

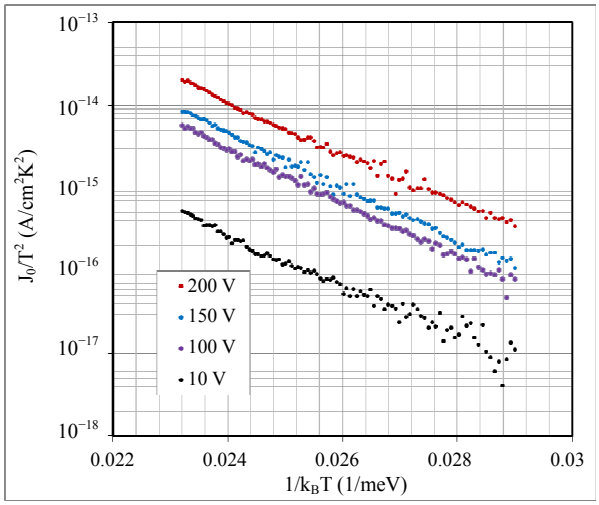

(a)

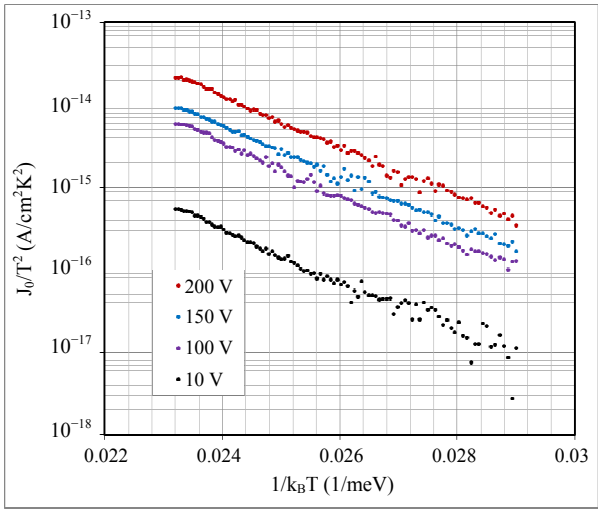

(b)

Figure 6. Arrhenius plots of J_0T^{-1} at various d.c. bias voltages, (a) during heating up and (b) during cooling down process.

Density J_0 of the current passing through the $Lu_3N@C_{80}$/Au structure at temperature of 450 K was plotted in **Figure 8** as a function of E. The reverse current J_0 does not saturate and increases slowly with increasing E from 0 to 0.4 MVm^{-1}. As shown in **Figure 7** there is not significant electric field dependence on the Schottky barrier. Therefore, the increase of J_0 with increasing electric field strength may be due to the tunneling effect of the carrier through the Schottky barrier and the carrier recombination in depletion layer. The bulk resistance decrease of the $Lu_3N@C_{80}$ solid phase can also result in the increase of J_0.

4. Discussion

4.1. Schottky Barrier and Energy Band Gap

Compared to the HOMO-LUMO energy gaps of C_{60} and

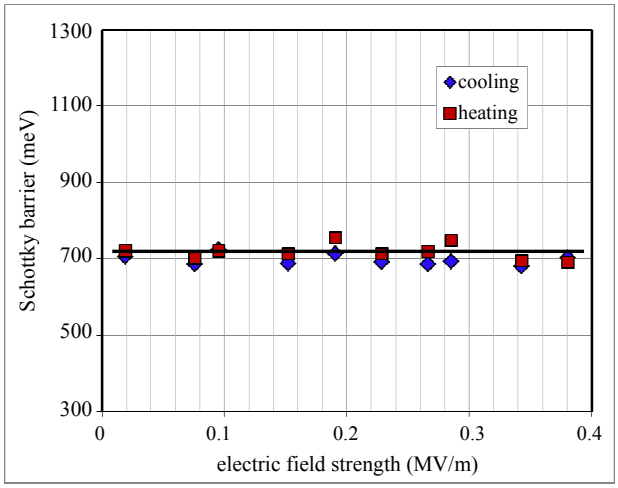

Figure 7. Schottky barrier of the $Lu_3N@C_{80}$/Au contact as a function of the electric field strength during heating up and cooling down process.

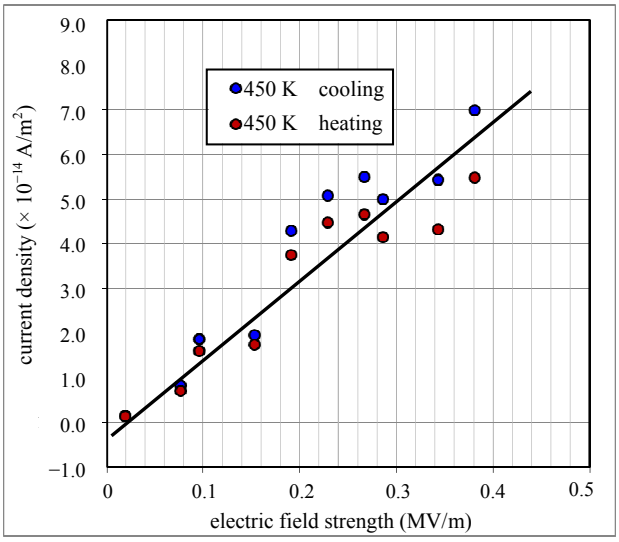

Figure 8. The density of the current passing through the $Lu_3N@C_{80}$/Au contact at temperature of 450 K as a function of the electric field strength during heating up and cooling down process.

C_{70} fullerenes, that of the C_{80} fullerene is small, 0.55 eV for D_2, 0,12 eV for I_h, 0.25 eV for D_{5d}, 0.12 eV for D_{5h}, 0.11 eV for $C_{2v'}$, 0.20 eV for D_3, and 0.11 eV for C_{2v} isomer. Except for the D_2 and D_{5d} isomers, the bare C_{80} isomers are unstable and still not be synthesized [6]. However, it is known that the encapsulation of the M_3N cluster makes them stable, and then the $M_3N@C_{80}$ molecule with I_h and D_{5h} symmetries can be stably extracted [7]. Electron transfer from the M_3N cluster to the C_{80} cage plays the most crucial role to the stability of the fullerenes with highly symmetrical geometries. Photoemission and x-ray absorption studies have indeed revealed that the C_{80} cages with I_h and D_{5h} symmetries are stabilized by the excessive electrons transferred from the M_3N cluster [1].

HOMO-LUMO energy gaps of anions and cations of C_{80} fullerene with the I_h symmetry have been calculated using *ab initio* molecular-orbital method [6]. It is 0.12 eV for neutral isomer, 0.38 eV for +2 cation, 0 eV for −2 anion, and 2.19 eV for −6 anion of the C_{80} isomer. On the other hand, theoretical calculations for the $[Lu_3N]^{+6}@[C_{80}]^{-6}$ molecule showed that its HOMO-LUMO energy gap is 1.54 - 2.55 eV [4,18]. Previous experimental studies also showed that the HOMO-LUMO gap of a $[Lu_3N]^{+6}@[C_{80}]^{-6}$ molecule is 1.31 - 1.65 eV [19,20] for optical absorption and 2.04 eV [4] for electrochemical measurement, respectively. In general, Schottky barrier of the semiconductor/metal is smaller than energy band gap of the semiconductor. In this study, the obtained Schottky barrier of the nanocrystalline $[Lu_3N]^{+6}@[C_{80}]^{-6}$ /Au contact is 0.71 ± 0.04 eV.

4.2. Electric Field Dependence of the Carrier Mobility

In general, the carrier mobility of fullerene crystals is very low due to impurity and poor crystallinity. For example, the electron drift mobility of C_{60} crystal is in the 1 $cm^2V^{-1}s^{-1}$ range and the hole mobility is smaller than that of electron in three orders of magnitude [21-23]. Sato *et al*. [24] have reported a study for measuring mobility of the $Sc_3N@C_{80}$ film with large grain size of several micrometers. The electron mobility of $Sc_3N@C_{80}$ film under room temperature and atmospheric pressure is 5.7×10^{-3} $cm^2V^{-1}s^{-1}$. The low mobility values indicate that the carrier propagation in the fullerene crystals is by hopping. The mobility in the order of 10^{-3} $cm^2V^{-1}s^{-1}$ gives a mean free path smaller than the molecular size, indicating that the band conduction model is not correct. A more likely mechanism of carrier transport in the fullerene solid would be hopping between grains or neighboring molecules. It is also reported that the carrier mobility of C_{60} crystal at temperatures above 300 K is independent of temperature [22,25].

We have discussed the free time dependence of the mobility above. From the electron mobility of $\mu_e = q\tau_c m_e^{*-1}$ where τ_c is the mean free time and m_e^* the electron effective mass, the mobility is also dependent of the effective mass m_e^*. If we assume that the mean free time τ_c of electron in the $Lu_3N@C_{80}$ solid phase is constant during measurements of the electric field dependence, the m_e^* depends only on the effective Richardson constant, $A^* = 4\pi q m_e^* k_B^2 h^{-3}$ where h is the Planck's constant. Therefore, the increase in the reverse saturation-current density J_0 as shown in **Figure 8** may be related to the increase in the electron effective mass m_e^* with increasing electric field.

4.3. Effects of the Adsorbed Oxygen Atoms

The XPS spectra of the $Lu_3N@C_{80}$ solid convey information of the thin surface layer within the depth of only 5 nm. Therefore, effects of the adsorbed oxygen atoms on the binding energies of C 1*s* and Lu 4 *d* are sensitively detected as seen in **Figure 3**. Due to the adsorption of oxygen atoms, the binding energy increases by 2 eV for the C 1*s* level and by 3 eV for the Lu 4 $d^{5/2}$ and $d^{3/2}$ levels, respectively. Compared to the Schottky barrier of the $Lu_3N@C_{80}$ solid, the shifts of the C and Lu-related levels are large. However, in this study the effect of impurity oxygen atoms on the measurement of the Schottky barrier of the $Lu_3N@C_{80}$ solid phase can be ignored because of a small concentration or a just physical adsorption of oxygen atoms.

4.4. Interaction between the Applied Electric Field and the Dipoles in $Lu_3N@C_{80}$ Molecule

The M_3N cluster can adopt ten equivalent orientations in the C_{80} cage by aligning its C_3 axis to ten different C_3 axes of the C_{80} cage. For each orientation, the cluster can occupy four equivalent positions with different azimuths corresponding to the rotation about its C_3 axis. Popov *et al*. [26] reported a calculation of molecular orientational dynamics of the Lu_3N cluster in the C_{80} cage. A thermal activation behavior of the cluster rotation appears, strongly depending on the cluster orientation with respect to the C_{80} cage. The barriers to the cluster rotation with respect to the C_3 axes of the C_{80} cage are below 155 meV, and have a minimum closing to zero at room temperature. The barriers to the cluster rotation inside the C_{80} cage are also found to somewhat increase in the charged states [26]. It is well known that there are dipoles in the M_3N cluster due to the electron transfer from metal atoms to nitrogen atoms [27]. However, no coupling between the applied electric field and the dipoles in the M_3N cluster is observed in this study. This is due to a high symmetry of three dipoles in the Lu_3N molecule as well as a screening effect of both the high-speed rotating C_{80} cage and the excessive electrons on it.

High-speed rotation of the $Lu_3N@C_{80}$ molecule at room temperature have a high relaxation rate due to the enlarged cage size, the excessive electrons as well as the additional dipole-dipole interaction between the endohedral cluster and the C_{80} cage, compared with the empty fullerenes such as C_{60} and C_{70} [12,28]. Furthermore, polarizations of the $M_3N@C_{80}$ molecule have been reported and its polarizability increases with increasing molecular diameter [27]. In order to estimate the influence of the $M_3N@C_{80}$ molecular polarization, we can calculate the potential energy of a dipole with elementary charge on the C_{80} cage by using $U = -qE\delta$ where q is the elementary charge, E the strength of applied electric field and δ the diameter of the C_{80} cage. We have the potential energy of the $Lu_3N@C_{80}$ molecule having the dipole with elementary charge, $U = -qE\delta$ meV where diameter of the C_{80} cage is 1 nm and the maximum electric field strength used in this study is 0.4 MVm^{-1}. It is clear that the potential energy is much smaller than the mean kinetic energy of a molecule, $3k_BT/2 = 39$ meV at room temperature. Therefore, even there is a dipole in the $Lu_3N@C_{80}$ molecule, its polarization effect cannot be observed due to strong thermal rotation and diffusion motions of the molecule.

Similar to the results of polarization effects of the endohedral Lu_3N cluster, we can also conclude that polarization effects of the $Lu_3N@C_{80}$ molecule can be ignored under the condition of the electric field strength used in this study, thus the capacitance or the Schottky barrier of the $Lu_3N@C_{80}$/Au contact is independent of applied electric field.

5. Conclusion

We have studied the structural properties of the nanocrystalline $Lu_3N@C_{80}$ fullerene solid with fcc structure by x-ray photoemission spectroscopy and x-ray diffraction measurement. The current-voltage characteristics of the $Lu_3N@C_{80}$/Au Schottky contact were measured at various electric fields and temperatures. The Schottky barrier of the $Lu_3N@C_{80}$/Au contact is estimated to be 0.71 ± 0.04 eV and the effect from the applied electric field can be ignored. The interaction between the applied electric field and the dipoles in the endohedral Lu_3N cluster and the C_{80} cage cannot be observed.

6. Acknowledgements

We are grateful to Professor Akira Namiki for fruitful discussions and valuable comments. This work was partially supported by project No. 15-B01, Program of Research for the Promotion of Technological Seeds, Japan Science and Technology Agency (JST). It was also partially supported by Grant-in-Aid for Exploratory Research No: 23651115, Japan Society for the Promotion of Science (JSPS).

REFERENCES

[1] S. Stevenson, G. Rice, T. Glass, K. Harich, F. Cromer, M. Jordan, J. Craft, E. Hadju, R. Bible, M. Olmstead, K. Maitra, A. Fisher, A. Balch and H. Dorn, "Small-Band-gap Endohedral Metallofullerenes in High Yield and Purity," *Nature* (*London*), Vol. 401, No. 6748, 1999, pp. 55-57. http://dx.doi.org/10.1038/43415

[2] L. Dunsch, M. Krause, J. Noack and P. Georgi, "Endohedral Nitride Cluster Fullerenes: Formation and Spectroscopic Analysis of $L_{3-x}M_xN@C_{2n}$ ($0 \le x \le 3$; N=39,40)," *Journal of Physics and Chemistry of Solids*, Vol. 65, No.

2-3, 2004, pp. 309-315. http://dx.doi.org/10.1016/j.jpcs.2003.03.002

[3] S. F. Yang, M. Kalbac, A. Popov and L. Dunsch, "Gadolinium-Based Mixed-Metal Nitride Clusterfullerenes $Gd_xSc_{3-x}N@C_{80}$ (x=1, 2)," *ChemPhysChem*, Vol. 7, No. 9, 2006, pp. 1990-1995. http://dx.doi.org/10.1002/cphc.200600323

[4] T. Cai, L. Xu, M. R. Anderson, Z. Ge, T. Zuo, X. Wang, M. M. Olmstead, A. L. Baich, H. W. Gibson and H. C. Dom, "Structure and Enhanced Reactivity Rates of the D_{5h} $Sc_3N@C_{80}$ and $Lu_3N@C_{80}$ Metallofullerene Isomers: The Importance of the Pyracylene Motif," *Journal of the American Chemical Society*, Vol. 128, No. 26, 2006, pp. 8581-8189. http://dx.doi.org/10.1021/ja0615573

[5] H. W. Kroto, "The Stability of the Fullerenes C_n, with n = 24, 28, 32, 36, 50, 60 and 70," *Nature*, Vol. 329, No. 6139, 1987, pp. 529-531. http://dx.doi.org/10.1038/329529a0

[6] K. Nakao, N. Kurita and M. Fujita, "*Ab initio* Molecular-Orbital Calculation for C_{70} and Seven Isomers of C_{80}," *Physical Review B*, Vol. 49, No. 16, 1994, pp. 11415-11420. http://dx.doi.org/10.1103/PhysRevB.49.11415

[7] M. Krause and L. Dunsch, "Isolation and Characterisation of Two $Sc_3N@C_{80}$ Isomers," *ChemPhysChem*, Vol. 5, No. 9, 2004, pp. 1445-1449. http://dx.doi.org/10.1002/cphc.200400085

[8] B. Larade, J. Talor, Q. R. Zheng, H. Mehrez, P. Pomorski and H. Guo, "Renormalized Molecular Levels in a $Sc_3N@C_{80}$ Molecular Electronic Device," *Physical Review B*, Vol. 64, No. 19, 2001, Article ID: 195402.

[9] T. R. Cummins, M. Burk, M. Schmidt, J. F. Armbruster, D. Fuchs, P. Adelmann, S. Schuppler, R. H. Michel and M. M. Kappes, "Electronic States and Molecular Symmetry of the Higher Fullerene C_{80}," *Chemical Physics Letters*, Vol. 261, No. 3, 1996, pp. 228-233. http://dx.doi.org/10.1016/0009-2614(96)00973-6

[10] A. Muller, S. Schippers, R. A. Phaneuf, M. Habibi, D. Esteves, J. C. Wang, A. L. D. Kilcoyne, A. Aguilar, S. Yang and L. Dunsch, "Photoionization of the Endohedral Fullerene Ions $Sc_3N@C_{80}^+$ and $Ce@C_{82}^+$ by Synchrotron Radiation," *Journal of Physics*: *Conference Series*, Vol. 88, 2007, Article ID: 012038. http://dx.doi.org/10.1088/1742-6596/88/1/012038

[11] M. Krause, H. Kuzmany, P. Georgi, L. Dunsch, K. Vietze and G. Seifert, "Structure and Stability of Endohedral Fullerene $Sc_3N@C_{80}$: A Raman, Infrared, and Theoretical Analysis," *Journal of Chemical Physics*, Vol. 115, 2001, pp. 6596-6605. http://dx.doi.org/10.1063/1.1399298

[12] S. Klod, L. Zhang and L. Dunsch, "The Role of the Cluster on the Relaxation of Endohedral Fullerene Cage Carbons: A NMR Spin-Lattice Relaxation Study of an Internal Relaxation Reagent," *Journal of Physical Chemistry C*, Vol. 114, No. 18, 2010, pp. 8264-8267. http://dx.doi.org/10.1021/jp101218p

[13] T. Huang, J. Zhao, M. Feng, H. Petek, S. Yang and L. Dunsch, "Superatom Orbitals of $Sc_3N@C_{80}$ and Their Tntermolecular Hybridization on Cu(110)-(2×1)-O Surface," *Physical Review B*, Vol. 81, No. 8, 2010, Article ID: 085434. http://dx.doi.org/10.1103/PhysRevB.81.085434

[14] L. Xu, S. F. Li, L. H. Gan, C. Y. Shu and C. R. Wang, "The Structures of Trimetallic Nitride Fullerenes $M_3N@C_{88}$: Theoretical Evidence of Corporation between Electron Transfer Interaction and Size Effect," *Chemical Physics Letters*, Vol. 521, 2012, pp. 81-85. http://dx.doi.org/10.1016/j.cplett.2011.11.011

[15] L. Chen, E. E. Carpenter, C. S. Hellberg, H. C. Dorn, M. Shultz, W. Wernsdorfer and I. Chiorescu, "Spin Transition in $Gd_3N@C_{80}$, Detected by Low-Temperature on-chip SQUID Technique," *Journal of Applied Physics*, Vol. 109, 2011, Article ID: 07B101.

[16] M. Wolf, K. H. Muller, D. Eckert, Y. Skourski, P. Georgi, R. Marczak, M. Krause and L. Dunsch, "Magnetic Moments in $Ho_3N@C_{80}$ and $Tb_3N@C_{80}$," *Journal of Magnetism and Magnetic Materials*, Vol. 290-291, 2005, pp. 290-293. http://dx.doi.org/10.1016/j.jmmm.2004.11.211

[17] M. E. Plonska-Brzezinska, A. J. Athans, J. P. Phillips, S. Stevenson and L. Echegoyen, ". A Reinvestigation of the Electrochemical Behavior of $Sc_3N@C_{80}$," *Journal of Electroanalytical Chemistry*, Vol. 614, No. 1-2, 2008, pp. 171-174. http://dx.doi.org/10.1016/j.jelechem.2007.11.013

[18] Y. Zhu, Y, Li and Z. Q. Yang, "First-Principles Investigation on the Electronic Structures of Intercalated Fullerenes $M_3N@C_{80}$ (M=Sc, Y, and lanthanides)," *Chemical Physics Letters*, Vol. 461, No. 4-6, 2008, pp. 285-289. http://dx.doi.org/10.1016/j.cplett.2008.07.045

[19] S. Stevenson, H. M. Lee, M. M. Olmstead, C. Kozikowski, P. Stevenson and A. L. Balch, "Preparation and Crystallographic Characterization of a New Endohedral, $Lu_3N@C_8$ 5 (*o*-xylene), and Comparison with $Sc_3N@C_{80}$ 5 (*o*-xylene)," *Chemistry—A European Journal*, Vol. 8, No. 19, 2002, pp. 4528-4535. http://dx.doi.org/10.1002/1521-3765(20021004)8:19<4528::AID-CHEM4528>3.0.CO;2-8

[20] E. B. Iezzi, J. C. Duchamp, K. R. Fletcher, T. E. Glass and H. C. Dorn, "Lutetium-Based Trimetallic Nitride Endohedral Metallofullerenes: New Contrast Agents," *Nano Letters*, Vol. 2, No. 11, 2002, pp. 1187-1190. http://dx.doi.org/10.1021/nl025643m

[21] R. Konenkamp, G. Priebe and B. Pietzak, "Carrier Mobilities and Influence of Oxygen in C_{60} Films," *Physical Review B*, Vol. 60, No. 16, 1999, pp. 11804-11808. http://dx.doi.org/10.1103/PhysRevB.60.11804

[22] E. Frankevich, Y. Maruyama and H. Ogata, "Mobility of Charge Carriers in Vapor-Phase Grown C_{60} Single Crystal," *Chemical Physics Letters*, Vol. 214, No. 1, 1993, pp. 39-44. http://dx.doi.org/10.1016/0009-2614(93)85452-T

[23] G. Priebe, B. Pietzak and R. Konenkamp, "Determination of Transport Parameters in Fullerene Films," *Applied Physics Letters*, Vol. 71, 1997, pp. 2160-2162. http://dx.doi.org/10.1063/1.119368

[24] S. Sato, S. Seki, G. Luo, M. Suzuki, J. Lu and S. Nagase, "Tunable Charge-Transport Properties of I_h-C_{80} Endohedral Metallofullerenes: Investigation of $La_2@C_{80}$, $Sc_3N@C_{80}$, and $Sc_3C_2@C_{80}$," *Journal of the American Chemical Society*, Vol. 134, No. 28, 2012, pp. 11681-11686. http://dx.doi.org/10.1021/ja303660g

[25] E. Frankevich, Y. Maruyama and H. Ogata, "Mobilities of Charge Carriers in C_{60} Orthorhombic Single Crystal," *Solid State Communications*, Vol. 88, 1993, pp. 177-181.

[26] A. A. Popov and L. Dunsch, "Hindered Cluster Rotation and ^{45}Sc Hyperfine Splitting Constant in Distonoid Anion Radical $Sc_3N@C_{80}^-$, and Spatial Spin-Charge Separation as a General Principle for Anions of Endohedral Fullerenes with Metal-Localized Lowest Unoccupied Molecular Orbitals," *Journal of the American Chemical Society*, Vol. 130, No. 52, 2008, pp. 17726-17742. http://dx.doi.org/10.1021/ja804226a

[27] J. He, K. Wu, R. Sa, Q. Li and Y. Wei, "Dipole Polarizabilities of Trimetallic Nitride Endohedral Fullerenes $M_3N@C_{2n}$ (M=Sc and Y; $2n$=68 – 98)," *Chemical Physics Letters*, Vol. 475, No. 1-3, 2009, pp. 73-77. http://dx.doi.org/10.1016/j.cplett.2009.05.010

[28] S. Klod and L. Dunsch, "Influence of the Cage Size on the Dynamic Behavior of Fullerenes: A Study of ^{13}C NMR Spin-Lattice Relaxation," *ACS NANO*, Vol. 4, No. 6, 2010, pp. 3236-3240. http://dx.doi.org/10.1021/nn1002024